bridgehead atom to allow extensive delocalization.

However, the present study shows that for the analogous complexes where the bridgehead atom is carbon (i.e. X = COH in the title complex, and X = CH[10]) the cyclic voltammetric behavior parallels that of $Co(bpy)_3^{n+}$ and not $Co\{(2\text{-}py)_3N\}_2^{n+}$. Furthermore, there is evidence from the coulometric studies reported above for the transient existance of the $[Co\{(2\text{-}py)_3COH\}_2]^+$, and the $[Co\{(2\text{-}py)_3CH\}_2]^+$ complex can be synthesized by sodium amalgam reduction of the Co(II) species and shows reasonable stability (several days) under inert conditions.[10a] Since delocalization via $d\pi$–$p\pi$ bonding would not be anticipated in either of these ligands, the above observations argue against the necessity of extensive delocalization via the bridging atom to allow stabilization of the low-valent Co(I) species, unless there is a spatial electronic interaction between pyridine rings in these tripodal ligands.[28]

Further studies of the Co(I) and Rh(I) complexes of a number of these tripodal ligands are in progress[10b] and will be reported subsequently.

Acknowledgment. This research was performed partly at Brookhaven National Laboratory (which is operated under Contract No. DE-AC02-76CH00016 with the Department of Energy and supported in part by its Office of Basic Energy Sciences) and partly at James Cook University of North Queensland (where it was supported by the Australian Research Grants Scheme). D.J.S. thanks Baruch College for released time to do this research, and F.R.K. acknowledges the Australian-American Educational Foundation for assistance through a Fulbright Award while on a Special Studies Program at Brookhaven National Laboratory. The contribution of Tracy Wilson (an undergraduate student at James Cook University) to aspects of the solvent dependence of linkage isomer formation is also acknowledged.

Registry No. $[Co\{(2\text{-}py)_3COH\}\{(2\text{-}py)_3CO^-\}](ClO_4)_2$, 73580-28-6; $[Co\{(2\text{-}py)_3COH\}_2](ClO_4)_3$, 102630-75-1; $Li[Co\{(2\text{-}py)_3COH\}_2](S_2O_6)_2\cdot 10H_2O$, 102630-77-3.

Supplementary Material Available: Tables of thermal parameters for the non-hydrogen atoms, positional parameters for the hydrogen atoms, interatomic distances and angles for the ligand, the anions, and the lithium coordination sphere, hydrogen bonding interactions, and least-squares planes (9 pages). Ordering information is given on any current masthead page.

(28) In this case, the complex of tris(2-pyridyl)amine may be the exception because of ligand distortion induced by the relative shortness of the bridgehead (N)–pyridine bonds.

(29) The periodic group notation in parentheses is in accord with recent actions by IUPAC and ACS nomenclature committees. A and B notation is eliminated because of wide confusion. Groups IA and IIA become groups 1 and 2. The d-transition elements comprise groups 3 through 12, and the p-block elements comprise groups 13 through 18. (note that the former Roman number designation is preserved in the last digit of the new numbering: e.g., III → 3 and 13).

Contribution from the Departments of Chemistry, Rice University, Houston, Texas 77251, University of Houston, Houston, Texas 77004, and The State University of New York at Buffalo, Buffalo, New York 14214

Structural and Theoretical Discussion of $[Bi_4Fe_4(CO)_{13}]^{2-}$: Application of MO and TEC Theories to a Zintl–Metal Carbonylate

Kenton H. Whitmire,*† Thomas A. Albright,*‡ Sung-Kwon Kang,‡ Melvyn Rowen Churchill,*§ and James C. Fettinger§

Received December 2, 1985

The reaction of $[Et_4N][BiFe_3(CO)_{10}]$ with CO in CH_2Cl_2 cleanly produces $[Et_4N]_2[Bi_4Fe_4(CO)_{13}]$ and iron pentacarbonyl. The complex crystallizes in the centrosymmetric orthorhombic space group *Pcab* (No. 61), with a = 14.128 (3) Å, b = 15.567 (4) Å, c = 39.816 (18) Å, V = 8756 (5) Å^3, and D(calcd) = 2.55 g cm^{-3} for Z = 8 and M_r = 1683.96. Diffraction data (Mo Kα, 2θ = 6–40°) were collected with a Syntex $P2_1$ automated diffractometer; the structure was solved and refined to R_F = 7.8% for those 2926 reflections with $|F_o| > 3.0\sigma(|F_o|)$. The $[Bi_4Fe_4(CO)_{13}]^{2-}$ dianion can be described as a hybrid Zintl ion–metal carbonyl, with three $Fe(CO)_3$ units capping faces of a Bi_4 tetrahedron. An additional $Fe(CO)_4$ fragment is apically bonded to that unique bismuth atom which is bonded to all three $Fe(CO)_3$ units. The $[Bi_4Fe_4(CO)_{13}]^{2-}$ dianion is involved in some significant intermolecular Bi–Bi contacts. Molecular orbital calculations have been carried out and are discussed along with qualitative electron-counting formalisms.

Introduction

The interest in metal cluster chemistry has dramatically increased during the last decade. The structures, the nature of the bonding, and the reactivity of metal cluster compounds are generally well established by synthetic, spectroscopic, and theoretical studies.[1-3] There are a number of transition-metal complexes that contain A_3 or A_4 groups, where A is phosphorus or arsenic, bonded to the transition-metal atoms. Most of the complexes show η^3-A_3–ML_3, η^3-A_3–M_2L_6 and η^1,η^2-A_4–ML_3 geometries.[4] Among the group 15 elements, unfortunately, bismuth–transition-metal cluster chemistry is not well-known. A few cationic or anionic polybismuth clusters have been known for some time,[5] and a few organic derivatives containing Bi–Bi bonds have also been reported recently.[6]

A preliminary account of the structure of a $[Bi_4Fe_4(CO)_{13}]^{2-}$ cluster compound has appeared[7] and has encouraged us to undertake MO studies to understand the bonding in it. This cluster compound is an electron-rich Zintl–metal carbonylate that is based on a p-block cluster framework. The complete structural details

† Rice University.
‡ University of Houston.
§ The State University of New York at Buffalo.

(1) (a) McPartlin, M.; Mingos, D. M. P. *Polyhedron* **1984**, *3*, 1321. (b) Teo, B. K. *Inorg. Chem.* **1984**, *23*, 1251. (c) Teo, B. K.; Longoni, G.; Chung, F. R. K. *Inorg. Chem.* **1984**, *23*, 1257. (d) Johnson, B. F. G. *Transition Metal Clusters*; Wiley-Interscience: Chichester, England, 1980. (e) Nicholls, J. N. *Polyhedron* **1984**, *3*, 1307.

(2) Burdett, J. K. *Molecular Shapes*; Wiley-Interscience: New York, 1980.

(3) Albright, T. A.; Burdett, J. K.; Whangbo, M.-H. *Orbital Interactions in Chemistry*; Wiley: New York, 1985.

(4) (a) Dapporto, P.; Sacconi, L.; Stoppioni, P.; Zanobini, F. *Inorg. Chem.* **1981**, *20*, 3834. (b) Bianchini, C.; Mealli, C.; Meli, A.; Sacconi, L. *Inorg. Chim. Acta* **1979**, *37*, L543. (c) Dapporto, P.; Middollini, S.; Sacconi, L. *Angew. Chem., Int. Ed. Engl.* **1979**, *18*, 469. (d) DiVaira, M.; Sacconi, L. *Angew. Chem., Int. Ed. Engl.* **1982**, *21*, 330. (e) Lindsell, W. E.; McCullough, K. J.; Welch, A. J. *J. Am. Chem. Soc.* **1983**, *105*, 4487. (f) DiVaira, M.; Midollini, S.; Sacconi, L. *J. Am. Chem. Soc.* **1979**, *101*, 1757. (g) Bernal, I.; Brunner, H.; Meier, W.; Pfisterer, H.; Wachter, J.; Ziegler, M. L. *Angew. Chem., Int. Ed. Engl.* **1984**, *23*, 4381. (h) DiVaira, M.; Mani, F.; Moneti, S.; Peruzzini, M.; Sacconi, L.; Stoppioni, P. *Inorg. Chem.* **1985**, *24*, 2230.

(5) (a) Corbett, J. D. *Prog. Inorg. Chem.* **1976**, *21*, 129. (b) Adolphson, D. G.; Corbett, J. D.; Merryman, D. J. *J. Am. Chem. Soc.* **1976**, *98*, 7234. (c) Cisar, A.; Corbett, J. D. *Inorg. Chem.* **1977**, *16*, 2482. (d) Critchlow, S. C.; Corbett, J. D. *Inorg. Chem.* **1982**, *21*, 3286.

0020-1669/86/1325-2799$01.50/0

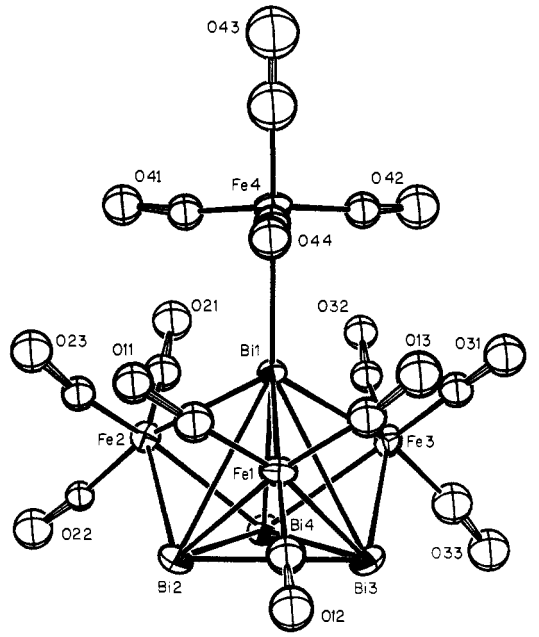

Figure 1. Labeling of atoms in the $[Bi_4Fe_4(CO)_{13}]^{2-}$ dianion. Note the approximate C_{3v} symmetry of the system.

and results from these theoretical considerations are presented here.

Results and Discussion

Synthesis and Structure of $[Et_4N]_2[Bi_4Fe_4(CO)_{13}]$ (I). This molecule is obtained via the reaction of carbon monoxide with the cluster $[Et_4N][(\mu_3\text{-Bi})Fe_3(CO)_9(\mu_3\text{-CO})]$ (II) in CH_2Cl_2 and can be easily obtained under moderate pressures (500 psi).[7] The cluster is obtained from the autoclave reaction in roughly 35% yield based on bismuth. It has been isolated as a minor product from the synthesis of $[BiFe_3(CO)_{10}]^-$ (probably because carbon monoxide is present as a byproduct of that reaction) and can be obtained along with $Fe(CO)_4PPh_3$ and $Fe(CO)_3(PPh_3)_2$ when $[BiFe_3(CO)_{10}]^-$ is treated with PPh_3 in CH_2Cl_2. The molecular structure of I is shown in Figure 1.

The crystal consists of a 2:1 ratio of disordered Et_4N^+ ions[9] (centered on N(1) and N(2)) and ordered $[Bi_4Fe_4(CO)_{13}]^{2-}$ dianions. The labeling of atoms within a $[Bi_4Fe_4(CO)_{13}]^{2-}$ ion is shown in Figure 1. A stereoscopic view of the cluster is provided in Figure 2. Interatomic distances and angles are listed in Tables III and IV.

The four bismuth atoms define a tetrahedron in which three triangular faces are capped by μ_3-$Fe(CO)_3$ fragments, while the fourth triangular face is bare. Bi–Bi distances around the bare face [Bi(2)–Bi(3) = 3.162 (2), Bi(3)–Bi(4) = 3.168 (2), Bi(4)–Bi(2) = 3.140 (2) Å] are systematically reduced by about 0.3 Å relative to the other three Bi–Bi distances within the Bi_4 core of the anion [viz., Bi(1)–Bi(2) = 3.473 (2), Bi(1)–Bi(3) = 3.473 (2), Bi(1)–Bi(4) = 3.453 (2) Å]. The μ_3-$Fe(CO)_3$ fragments are linked to the Bi_4 tetrahedron such that the Bi(1)–Fe linkages are slightly shorter than the other two Bi–Fe distances in each case (viz., Bi(1)–Fe(1) = 2.708 (5) Å vs. Bi(2)–Fe(1) = 2.753 (6) and Bi(3)–Fe(1) = 2.736 (6) Å; Bi(1)–Fe(2) = 2.699 (6) Å vs. Bi(2)–Fe(2) = 2.733 (5) and Bi(4)–Fe(2) = 2.729 (6) Å; Bi(1)–Fe(3) = 2.701 (6) Å vs. Bi(3)–Fe(3) = 2.714 (6) and Bi(4)–Fe(3) = 2.729 (6) Å). The fourth iron atom is the central atom of an $Fe(CO)_4$ unit that is linked only to the apical Bi(1), with Bi(1)–Fe(4) = 2.752 (6) Å. Atoms Fe(1), Fe(2), and Fe(3) are each in a distorted-octahedral coordination environment, whereas Fe(4) has a trigonal-bipyramidal geometry. The $[Bi_4Fe_4(CO)_{13}]^{2-}$ cluster as a whole has approximate C_{3v} symmetry.

Other distances and angles within the $[Bi_4Fe_4(CO)_{13}]^{2-}$ anion are in agreement with known values but are of limited precision because of the dominance of the heavy atoms (i.e., four bismuth atoms with $Z = 83$ and four iron atoms with $Z = 26$) in the X-ray structural analysis. Thus Fe–CO distances are 1.61 (8)–1.80 (6) Å (average, 1.72 ± 0.06 Å), C–O distances are 1.11 (6)–1.31 (6) Å (average, 1.19 ± 0.06 Å) and Fe–C–O angles are 169 (4)–179 (4)° (average, 174 ± 3°).

The two Bi–Bi distances observed for I (ca. 3.16 and 3.46 Å) are comparable with the two closest Bi–Bi contacts in the pure crystalline element (3.07 and 3.53 Å).[10] Compound I may be compared to the Bi_4^{2-} anion, which has been crystallographically characterized.[5c] In this molecule, a square-planar array of Bi atoms is observed with two unique Bi–Bi distances of 2.936 (2) and 2.941 (2) Å. These distances are noticeably shorter than for I, and this may arise via π interactions in the square-planar molecule since it is an aromatic 6-π-electron system. Unfortunately, the Bi–Bi distances cannot be directly compared to these in tetrahedral $Sn_2Bi_2^{2-}$ since in the latter molecule the Sn and Bi atoms are equally disordered over all sites.[5d] The Bi–Bi distance in the cationic cluster $Bi_8(AlCl_4)_2$ of 3.100 Å (average) compares favorably to the basal Bi–Bi distance in I and suggests that they represent a Bi–Bi single bond.[11] As shown in Figure 3, there are weak Bi...Bi interactions between the dianions. Close intercluster contacts observed in I (ca. 3.980 Å) are also comparable to those observed for Bi_8^{2+} at 3.900 (6)–4.109 (6) Å[11] and $Ca_{11}Bi_{10}$.[12] The longer Bi–Bi distances in I indicates appreciably weakened bonding as will be discussed in the next section.

Theoretical Considerations. In $[Bi_4Fe_4(CO)_{13}]^{2-}$ the one $Fe(CO)_4$ unit that is connected to only one Bi atom can be considered a two-electron acceptor. We assume that two electrons on the Bi atom, a lone pair of electrons directed toward the outside of the tetrahedral cage, are used to form a dative bond to the $Fe(CO)_4$ group and the skeletal bonding in the cluster compound will not be affected by this interaction. Therefore, the model for our studies does not include the $Fe(CO)_4$ unit. Three $Fe(CO)_3$ moieties are coordinated in an μ_3 fashion to three faces of the Bi_4 tetrahedron. The nine Bi–Fe bonding distances are almost the

Table I. Experimental Data for the X-ray Diffraction Study of $[Et_4N]^+_2[Bi_4Fe_4(CO)_{13}]^{2-}$

(A) Crystal Parameters at 24 °C (297 K)

cryst syst: orthorhombic	V = 8756.4 (48) Å^3
space group: *Pcab* [No. 61]	Z = 8
a = 14.1276 (30) Å	formula: $C_{29}H_{40}N_2O_{13}Bi_4Fe_4$
b 15.5670 (37) Å	M_r = 1683.96
c = 39.816 (18) Å	D(calcd) = 2.55 g cm^{-3}

(B) Measurement of Intensity Data

diffractometer: Syntex $P2_1$
radiation: Mo K$\bar{\alpha}$ ($\bar{\lambda}$ = 0.710 730 Å)
monochromator: pyrolytic graphite ($2\theta_m$ = 12.160° for the 002 reflcn), equatorial mode, assumed 50% perfect/50% ideally mosaic for polarization cor
reflcns measd: $+h,+k,+l$ for 2θ = 6.0–40.0°; 4726 reflcns collcd, yielding 4072 unique data
scan type: ω–scan over a symmetrical range of 0.9° with an ofset of 0.5° for bkgd measurements
scan speed: 1.0°/min
std reflcns: 3 mutually orthogonal reflcns re-collcd after every 97 reflcns; no decay or significant fluctuations obsd
abs cor: μ(Mo Kα) = 165.9 cm^{-1}; an empirical abs cor made based upon interpolation (both in 2θ and ϕ) between ψ-scans of a set of close-to-axial reflcns

(6) (a) Breung, H. J.; Muller, D. *Angew. Chem.* **1982**, *94*, 448. (b) Ashe, A. J.; Ludwig, E. G. *Organometallics* **1982**, *1*, 1408. (c) Calderazzo, F.; Morvillo, A.; Pelizzi, G.; Poli, R. *J. Chem. Soc., Chem. Commun.* **1983**, 507.
(7) Whitmire, K. H.; Churchill, M. R.; Fettinger, J. C. *J. Am. Chem. Soc.* **1985**, *107*, 1056.
(8) Whitmire, K. H.; Lagrone, C. B.; Churchill, M. R.; Fettinger, J. C.; Biondi, L. V. *Inorg. Chem.* **1984**, *23*, 4227.
(9) Churchill, M. R.; Change, S. W.-Y. *Inorg. Chem.* **1974**, *13*, 2413.
(10) Curka, P.; Barrett, C. S. *Acta Crystallogr.* **1962**, *15*, 865.
(11) Krebs, B.; Hucke, M.; Brendel, C. J. *Angew. Chem., Int. Ed. Engl.* **1982**, *21*, 445.
(12) Deller, K.; Eisenmann, B. *Z. Naturforsch, B: Anorg. Chem., Org. Chem.* **1976**, *31*, 29.

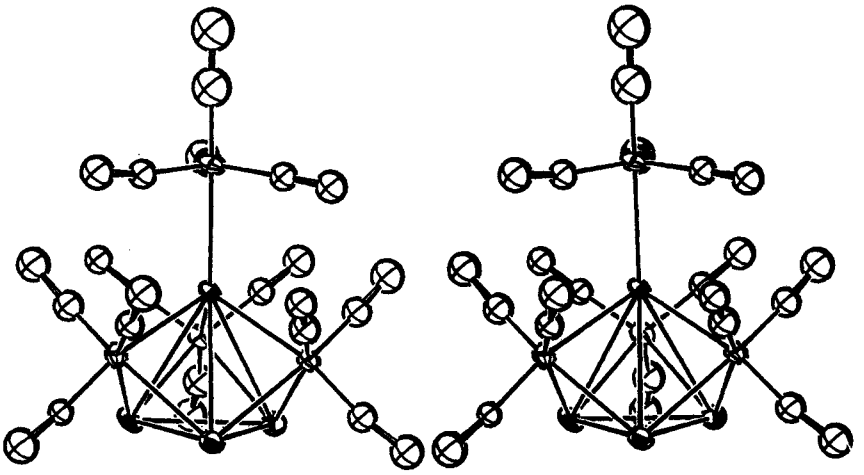

Figure 2. Stereoscopic view of the $[Bi_4Fe_4(CO)_{13}]^{2-}$ dianion.

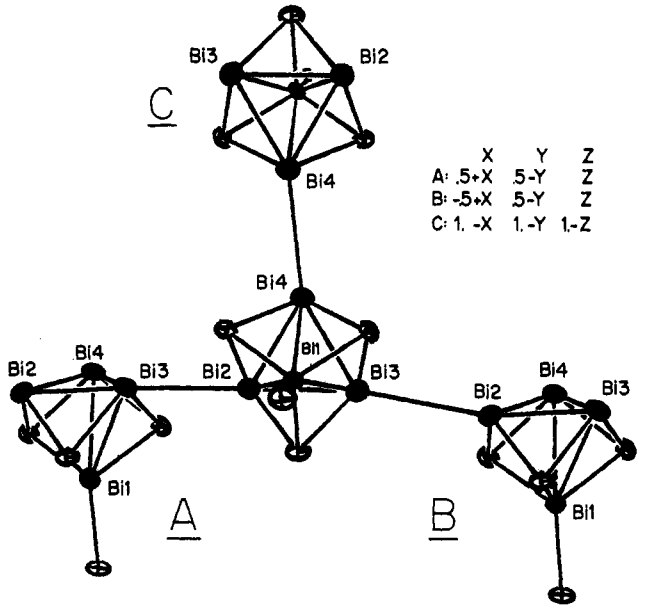

Figure 3. Interactions between the central and surrounding $[Bi_4Fe_4(CO)_{13}]^{2-}$ dianions. Note that all interactions involve the "bare" faces (Bi(2)–Bi(3)–Bi(4)) of the anions. Interionic distances <4 Å drawn in are Bi(2)–Bi(3,A) = Bi(3)–Bi(2,B) = 3.980 (2) Å and Bi(4)–Bi(4,C) = 3.981 (2) Å.

same, and the local symmetry around $Fe(CO)_3$ can be considered as C_{3v}. On the other hand, Bi–Bi distances show remarkable differences between basal and apical bond lengths, as noted earlier. Molecular orbital calculations using the extended Hückel method were carried out to probe these facets, but before we discuss the cluster compound, it is useful to derive the valence orbitals of the tetrahedral Bi_4 fragment.

The Bi_4 Fragment Orbitals. Bi_4 is a 20-electron tetrahedron. A number of related clusters are known, for example, P_4, As_4, Sb_4, Ge_4^{4-}, Sn_4^{4-}, Pb_4^{4-}, and $Sn_2Bi_2^{2-}$. Several theoretical studies have been done for such molecules to understand their bonding characteristics.[5d,13,14] We derived elsewhere[14i] general orbital

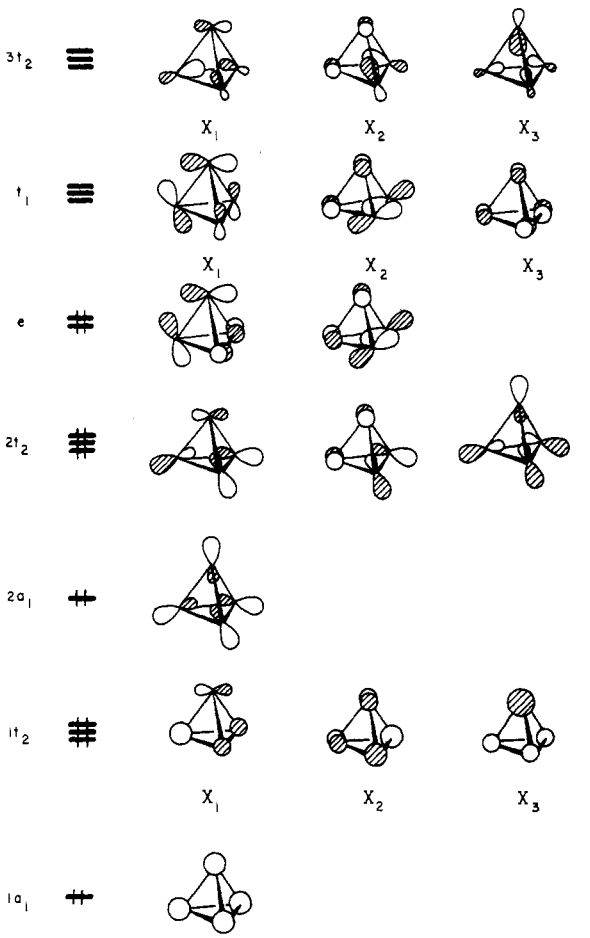

Figure 4. Important valence orbitals in the Bi_4 unit.

diagrams for the tetrahedron where one s and three p valence orbitals were considered at each atom. Thus, we shall only highlight the important features. The important valence orbitals in Bi_4 are shown in Figure 4. The $2a_1$ and $2t_2$ orbitals are filled, and they may be thought of as the lone pairs of the Bi atoms, pointed away from the vertices of the Bi_4 cage. The other six electron pairs will be used for cluster skeletal bonding. The filled $1a_1$, $1t_2$, and e orbitals result in six skeletal bonds in the Bi_4 cage. Considering Wade's rules,[14g] the total number of electron pairs for skeletal bonding is $n + 2$, where n is the number of vertices in the cluster, and thus the Bi_4 fragment will have a nido trigonal-bipyramidal geometry. Qualitatively, the ordering of valence orbitals in Bi_4 is identical with that in P_4, As_4, and Sb_4, which have been measured by photoelectron spectroscopy and computed by the semiempirical SCC Xα method.[14h] The reader should note that Bi_4 is a hypothetical fragment model in the cluster compound.

(13) Hart, R. R.; Robin, M. B.; Kuebler, N. A. *J. Chem. Phys.* **1965**, *42*, 3631.
(14) (a) Brundle, C. R.; Kuebler, N. A.; Robin, M. B.; Basch, H. *Inorg. Chem.* **1972**, *11*, 20. (b) Kettle, S. F. A. *Theor. Chim. Acta* **1966**, *4*, 150. (c) Archibald, R. M.; Perkins, P. G. *J. Chem. Soc. D* **1970**, 569. (d) Guest, M. F.; Hillier, I. H.; Saunders, V. R. *J. Chem. Soc., Faraday Trans. 2* **1972**, *68*, 2070. (e) Osman, R.; Coffey, P.; Van Wazer, J. R. *Inorg. Chem.* **1976**, *15*, 287. (f) Von Schnering, H.-G. *Angew. Chem., Int. Ed. Engl.* **1981**, *20*, 33. (g) Wade, K. *Adv. Inorg. Chem. Radiochem.* **1976**, *18*, 1. (h) Elbel, S.; Kudnig, J.; Grodzicki, M.; Lempka, H. J. *Chem. Phys. Lett.* **1984**, *109*, 312. (i) Kang, S.-K.; Albright, T. A.; Silvestre, J. *Croat. Chim. Acta* **1984**, *57*, 1355. (j) Elbel, S.; tom Dieck, H.; Walther, H.; Krizek, J. *Inorg. Chim. Acta* **1981**, *53*, L101.

Table II. Final Positional Parameters for $[Et_4N]^+_2[Bi_4Fe_4(CO)_{13}]^{2-}$

atom	x	y	z	B, Å²	atom	x	y	z	B, Å²
			(A) Atoms of the Polynuclear Dianion						
Bi(1)	0.46675 (10)	0.44648 (9)	0.38767 (4)		O(22)	0.7711 (23)	0.4295 (19)	0.4760 (10)	6.70 (82)
Bi(2)	0.59737 (11)	0.27713 (9)	0.42046 (5)		C(23)	0.6949 (29)	0.4514 (25)	0.3948 (12)	4.4 (10)
Bi(3)	0.37468 (12)	0.26452 (10)	0.42618 (5)		O(23)	0.7437 (22)	0.4605 (19)	0.3670 (10)	6.69 (79)
Bi(4)	0.48937 (11)	0.39516 (11)	0.47162 (4)		C(31)	0.2497 (32)	0.4268 (26)	0.4020 (14)	4.8 (10)
Fe(1)	0.47291 (39)	0.28053 (31)	0.36733 (16)		O(31)	0.1925 (23)	0.4320 (20)	0.3817 (10)	6.76 (82)
Fe(2)	0.62235 (37)	0.45047 (33)	0.42689 (16)		C(32)	0.3448 (26)	0.5416 (25)	0.4442 (12)	3.92 (93)
Fe(3)	0.33120 (38)	0.43280 (37)	0.43518 (16)		O(32)	0.3443 (18)	0.6156 (17)	0.45055 (83)	4.70 (65)
Fe(4)	0.45017 (46)	0.57347 (36)	0.33996 (17)		C(33)	0.2585 (36)	0.3970 (31)	0.4694 (16)	6.7 (12)
C(11)	0.5631 (32)	0.3021 (27)	0.3411 (14)	5.3 (11)	O(33)	0.2113 (23)	0.3793 (20)	0.4945 (10)	6.94 (85)
O(11)	0.6271 (19)	0.3219 (17)	0.32215 (85)	4.97 (68)	C(41)	0.5539 (31)	0.6116 (26)	0.3577 (13)	4.8 (10)
C(12)	0.4757 (29)	0.1717 (28)	0.3642 (13)	5.2 (10)	O(41)	0.6258 (22)	0.6436 (19)	0.36466 (93)	6.19 (76)
O(12)	0.4756 (20)	0.0952 (19)	0.35635 (92)	6.19 (76)	C(42)	0.3405 (30)	0.6003 (26)	0.3601 (13)	4.5 (10)
C(13)	0.3680 (32)	0.2972 (27)	0.3441 (14)	5.0 (11)	O(42)	0.2714 (24)	0.6229 (20)	0.3718 (10)	7.49 (90)
O(13)	0.3078 (23)	0.3101 (21)	0.3268 (10)	6.81 (82)	C(43)	0.4377 (46)	0.6469 (45)	0.3117 (21)	10.6 (19)
C(21)	0.5969 (32)	0.5539 (30)	0.4341 (14)	5.8 (11)	O(43)	0.4353 (31)	0.7045 (29)	0.2908 (14)	11.3 (13)
O(21)	0.5800 (22)	0.6319 (20)	0.4388 (10)	6.66 (81)	C(44)	0.4580 (27)	0.4887 (26)	0.3110 (12)	4.08 (92)
C(22)	0.7095 (26)	0.4330 (22)	0.4567 (11)	3.13 (81)	O(44)	0.4626 (19)	0.4327 (18)	0.29289 (89)	5.54 (70)
			(B) Atoms of the Disordered Et_4N^+ Cations						
N(1)	0.4843 (20)	0.3737 (18)	0.07511 (89)	3.22 (67)	C(22A)	0.1634	0.4331	0.2310	10.0
C(1A)	0.4160 (47)	0.3046 (42)	0.0753 (21)	2.6 (15)	C(21B)	0.3346	0.4234	0.2226	10.0
C(1B)	0.3827 (49)	0.3852 (43)	0.0781 (21)	3.2 (16)	C(23A)	0.2204	0.4642	0.2831	10.0
C(2)	0.3148 (35)	0.3215 (32)	0.0804 (15)	6.8 (13)	C(23B)	0.1526	0.5462	0.2891	10.0
C(3A)	0.5848 (43)	0.3456 (38)	0.0695 (19)	2.0 (14)	C(24A)	0.1957	0.5114	0.2138	10.0
C(3B)	0.4933 (60)	0.3321 (55)	0.0428 (27)	5.3 (22)	C(22B)	0.1115	0.3971	0.2529	10.0
C(4)	0.5954 (28)	0.3274 (25)	0.0299 (13)	4.4 (10)	C(24B)	0.1526	0.5835	0.2437	10.0
C(5A)	−0.012 (16)	0.687 (15)	0.3869 (70)	23.6 (84)	C(25A)	0.2398	0.4760	0.2203	10.0
C(5B)	0.4787 (77)	0.4048 (73)	0.1168 (35)	7.7 (29)	C(25B)	0.1639	0.4829	0.1936	10.0
C(6)	0.5202 (58)	0.3417 (58)	0.1381 (27)	13.6 (26)	C(26A)	0.1054	0.4594	0.2481	10.0
C(7A)	0.4494 (53)	0.4498 (48)	0.0534 (24)	4.1 (18)	C(26B)	0.0966	0.4163	0.2207	10.0
C(7B)	0.5383 (64)	0.4623 (57)	0.0804 (28)	5.5 (22)	C(27A)	0.2152	0.5242	0.2855	10.0
C(8)	0.5119 (35)	0.5337 (33)	0.0509 (16)	7.5 (14)	C(27B)	0.2916	0.5416	0.2986	10.0
N(2)	0.2153	0.4794	0.2470	10.0	C(28A)	0.1914	0.4305	0.2801	10.0
C(21A)	0.2729	0.3903	0.2492	10.0	C(28B)	0.2500	0.4583	0.3125	10.0

Table III. Final Interatomic Distances (Å) within the $[Bi_4Fe_4(CO)_{13}]^{2-}$ Dianion

	(A) Bi–Bi Distances		
Bi(1)–Bi(2)	3.473 (2)	Bi(2)–Bi(3)	3.162 (2)
Bi(1)–Bi(3)	3.473 (2)	Bi(2)–Bi(4)	3.140 (2)
Bi(1)–Bi(4)	3.453 (2)	Bi(3)–Bi(4)	3.168 (2)
	(B) Bi–Fe Distances		
Bi(1)–Fe(1)	2.708 (5)	Bi(2)–Fe(2)	2.733 (5)
Bi(1)–Fe(2)	2.699 (6)	Bi(3)–Fe(1)	2.736 (6)
Bi(1)–Fe(3)	2.701 (6)	Bi(3)–Fe(3)	2.714 (6)
Bi(1)–Fe(4)	2.752 (6)	Bi(4)–Fe(2)	2.729 (6)
Bi(2)–Fe(1)	2.753 (6)	Bi(4)–Fe(3)	2.729 (6)
	(C) Interionic Bi–Bi Distances (<4.0 Å)[a]		
Bi(2)–Bi(3,A)	3.980 (2)	Bi(4)–Bi(4,C)	3.981 (2)
Bi(3)–Bi(2,B)	3.980 (2)		
	(D) Fe–C and C–O Distances		
Fe(1)–C(11)	1.68 (5)	C(11)–O(11)	1.22 (6)
Fe(1)–C(12)	1.70 (4)	C(12)–O(12)	1.23 (5)
Fe(1)–C(13)	1.77 (5)	C(13)–O(13)	1.11 (6)
Fe(2)–C(21)	1.67 (5)	C(21)–O(21)	1.25 (6)
Fe(2)–C(22)	1.73 (4)	C(22)–O(22)	1.16 (5)
Fe(2)–C(23)	1.64 (5)	C(23)–O(23)	1.31 (6)
Fe(3)–C(31)	1.76 (5)	C(31)–O(31)	1.15 (6)
Fe(3)C(32)	1.74 (4)	C(32)–O(32)	1.18 (5)
Fe(3)–C(33)	1.80 (6)	C(33)–O(33)	1.23 (7)
Fe(4)–C(41)	1.73 (5)	C(41)–O(41)	1.17 (5)
Fe(4)–C(42)	1.79 (5)	C(42)–O(42)	1.14 (6)
Fe(4)–C(43)	1.61 (8)	C(43)–O(43)	1.22 (9)
Fe(4)–C(44)	1.76 (4)	C(44)–O(44)	1.13 (5)

[a] See Figure 3 for labeling of symmetry-related atoms.

The Bi_4 molecule has only been observed at elevated temperatures and is unknown in the solid state.

η^3-Bonding to a C_{3v} ML_3 Fragment. Metal complexes containing an A_4 group (A = group 15 element) bonded to ML_3 species in a η^3 fashion have not been synthesized. However, as mentioned in the Introduction, several complexes have been prepared and structurally determined for η^3-A_3–ML_n systems.

Figure 5 shows an interaction diagram for an ML_3 group bonded to a face in tetrahedral Bi_4. The valence MO's for the C_{3v} ML_3 system have been described in many places.[2,3] They are shown on the right side of the figure. The $1a_1$ and 1e set at low energy are pure metal orbitals which come from a t_{2g} set in an octahedral system. In the 2e set the orbitals are primarily metal d with some p character mixed in and are directed toward the Bi_4 fragment. The $2a_1$ orbital is primarily a metal s and p_z hybrid. The 2e set and $2a_1$ will form the largest interaction with Bi_4 because of their spatial extent. The total symmetry of the η^3-Bi_4–ML_3 system is C_{3v}. Therefore, the t_2 set of the tetrahedron is reduced to e + a_1, and t_1 is reduced to e + a_2. The X_2, X_3 components of $2t_2$ (actually an e set) and $2a_1$ on Bi_4 have a small interaction with the $1a_1$ and 1e set on ML_3 to produce the $1a_1$, 1e, $3a_1$, and 3e molecular orbitals. Since these orbitals are all occupied, the interactions will slightly destabilize the molecule by perturbation theory considerations.[3] The main sources for Bi–metal bonding are as follows: the 2e set on the ML_3 unit strongly interacts with the e set and X_1, X_2 components of t_1 on Bi_4. This gives the filled 2e and 4e and empty 5e molecular orbitals. The X_1 component in $2t_2$ is stabilized by $2a_1$ on the ML_3 unit to form the $2a_1$ MO. The $2a_1$ MO is not lowered much in energy because of another interaction with a lower lying metal fragment orbital, not shown in the figure. For a d^{10} metal system the 4e set is the HOMO, which is partially the result of a bonding interaction between the 2e set of ML_3 unit and X_1, X_2 in the t_1 set on Bi_4. Therefore, we anticipate appreciable metal back-bonding to the X_1 and X_2 components of the t_1 set. Since X_1 and X_2 are antibonding between each Bi atom, one would expect an elongation of the Bi–Bi bonds.

The Bi–Bi overlap population calculated for Bi_4 is 0.429; in $Bi_4FeL_3^{2-}$ the coordinated Bi–Bi overlap population is reduced to 0.319 while that between one coordinated Bi and the apical Bi atom was 0.349. Notice that there is a difference in the computed overlap populations for the complex. Accordingly, one

Table IV. Selected Angles (deg) within the $[Bi_4Fe_4(CO)_{13}]^{2-}$ Dianion

(A) Angles between Metal Atoms							
Bi(2)-Bi(1)-Bi(3)	54.16 (4)	Bi(3)-Bi(2)-Bi(4)	60.36 (5)	Fe(2)-Bi(4)-Fe(3)	98.59 (18)	Bi(2)-Bi(3)-Bi(4)	59.47 (5)
Bi(2)-Bi(1)-Bi(4)	53.92 (4)	Bi(3)-Bi(2)-Fe(1)	54.58 (12)	Bi(4)-Bi(1)-Fe(1)	93.80 (13)	Bi(2)-Bi(3)-Fe(1)	55.06 (12)
Bi(2)-Bi(1)-Fe(1)	51.08 (12)	Bi(3)-Bi(2)-Fe(2)	100.55 (13)	Bi(4)-Bi(1)-Fe(2)	50.89 (12)	Bi(2)-Bi(3)-Fe(3)	100.08 (14)
Bi(2)-Bi(1)-Fe(2)	50.68 (12)	Bi(4)-Bi(2)-Fe(1)	100.20 (13)	Bi(4)-Bi(1)-Fe(3)	50.88 (13)	Bi(4)-Bi(3)-Fe(1)	99.86 (13)
Bi(2)-Bi(1)-Fe(3)	93.09 (13)	Bi(4)-Bi(2)-Fe(2)	54.86 (13)	Bi(4)-Bi(1)-Fe(4)	147.44 (14)	Bi(4)-Bi(3)-Fe(3)	54.63 (13)
Bi(2)-Bi(1)-Fe(4)	148.21 (14)	Fe(1)-Bi(2)-Fe(2)	97.80 (17)	Fe(1)-Bi(1)-Fe(2)	99.73 (17)	Fe(1)-Bi(3)-Fe(3)	98.06 (18)
Bi(3)-Bi(1)-Bi(4)	54.44 (5)	Bi(1)-Bi(4)-Bi(2)	63.37 (5)	Fe(1)-Bi(1)-Fe(3)	99.05 (18)	Bi(1)-Fe(1)-Bi(2)	78.98 (16)
Bi(3)-Bi(1)-Fe(1)	50.71 (12)	Bi(1)-Bi(4)-Bi(3)	63.11 (5)	Fe(1)-Bi(1)-Fe(4)	118.74 (18)	Bi(1)-Fe(1)-Bi(3)	79.29 (16)
Bi(3)-Bi(1)-Fe(2)	93.93 (13)	Bi(1)-Bi(4)-Fe(2)	50.10 (12)	Fe(2)-Bi(1)-Fe(3)	100.05 (18)	Bi(2)-Fe(1)-Bi(3)	70.36 (14)
Bi(3)-Bi(1)-Fe(3)	50.26 (13)	Bi(1)-Bi(4)-Fe(3)	50.16 (13)	Fe(2)-Bi(1)-Fe(4)	116.91 (19)	Bi(1)-Fe(2)-Bi(2)	79.49 (16)
Bi(3)-Bi(1)-Fe(4)	149.15 (14)	Bi(2)-Bi(4)-Bi(3)	60.17 (5)	Fe(3)-Bi(1)-Fe(4)	118.69 (19)	Bi(1)-Fe(2)-Bi(4)	79.00 (16)
Bi(1)-Bi(2)-Bi(3)	62.93 (5)	Bi(2)-Bi(4)-Fe(2)	54.96 (13)	Bi(1)-Bi(3)-Bi(2)	62.91 (5)	Bi(2)-Fe(2)-Bi(4)	70.18 (14)
Bi(1)-Bi(2)-Bi(4)	62.72 (5)	Bi(2)-Bi(4)-Fe(3)	100.29 (14)	Bi(1)-Bi(3)-Bi(4)	62.45 (5)	Bi(1)-Fe(3)-Bi(3)	79.80 (17)
Bi(1)-Bi(2)-Fe(1)	49.94 (12)	Bi(3)-Bi(4)-Fe(2)	100.48 (13)	Bi(1)-Bi(3)-Fe(1)	50.00 (12)	Bi(1)-Fe(3)-Bi(4)	78.96 (16)
Bi(1)-Bi(2)-Fe(2)	49.82 (12)	Bi(3)-Bi(4)-Fe(3)	54.18 (13)	Bi(1)-Bi(3)-Fe(3)	49.94 (13)	Bi(3)-Fe(3)-Bi(4)	71.19 (15)
(B) M-M-CO Angles (M = Bi or Fe)							
Bi(1)-Fe(1)-C(11)	91.1 (16)	Bi(3)-Fe(1)-C(13)	92.1 (16)	Bi(4)-Fe(3)-C(32)	90.5 (14)	Bi(4)-Fe(2)-C(21)	92.5 (17)
Bi(1)-Fe(1)-C(12)	166.8 (16)	Bi(1)-Fe(3)-C(31)	86.7 (15)	Bi(4)-Fe(3)-C(33)	89.9 (18)	Bi(4)-Fe(2)-C(22)	89.6 (13)
Bi(1)-Fe(1)-C(13)	89.4 (16)	Bi(1)-Fe(3)-C(32)	89.5 (14)	Bi(1)-Fe(2)-C(21)	86.9 (17)	Bi(4)-Fe(2)-C(23)	160.6 (16)
Bi(2)-Fe(1)-C(11)	89.8 (16)	Bi(1)-Fe(3)-C(33)	164.2 (18)	Bi(1)-Fe(2)-C(22)	166.6 (13)	Bi(1)-Fe(4)-C(41)	83.9 (15)
Bi(2)-Fe(1)-C(12)	91.3 (16)	Bi(3)-Fe(3)-C(31)	89.9 (15)	Bi(1)-Fe(2)-C(23)	93.3 (15)	Bi(1)-Fe(4)-C(42)	86.1 (15)
Bi(2)-Fe(1)-C(13)	160.3 (16)	Bi(3)-Fe(3)-C(32)	160.1 (14)	Bi(2)-Fe(2)-C(21)	159.6 (17)	Bi(1)-Fe(4)-C(43)	178.4 (26)
Bi(3)-Fe(1)-C(11)	159.2 (17)	Bi(3)-Fe(3)-C(33)	86.0 (18)	Bi(2)-Fe(2)-C(22)	90.1 (13)	Bi(1)-Fe(4)-C(44)	84.7 (14)
Bi(3)-Fe(1)-C(12)	89.1 (16)	Bi(4)-Fe(3)-C(31)	157.9 (16)	Bi(2)-Fe(2)-C(23)	90.9 (15)		
(C) Fe-C-O Angles							
Fe(1)-C(11)-O(11)	177 (4)	Fe(2)-C(22)-O(22)	173 (4)	Fe(3)-C(32)-O(32)	173 (4)	Fe(4)-C(42)-O(42)	175 (4)
Fe(1)-C(12)-O(12)	169 (4)	Fe(2)-C(23)-O(23)	171 (4)	Fe(3)-C(33)-O(33)	174 (5)	Fe(4)-C(43)-O(43)	175 (6)
Fe(1)-C(13)-O(13)	173 (4)	Fe(3)-C(31)-O(31)	172 (4)	Fe(4)-C(41)-O(41)	169 (4)	Fe(4)-C(44)-O(44)	179 (4)
Fe(2)-C(21)-O(21)	178 (4)						
(D) C-Fe-C Angles							
C(11)-Fe(1)-C(12)	98 (2)	C(21)-Fe(2)-C(23)	105 (2)	C(32)-Fe(3)-C(33)	102 (2)	C(42)-Fe(4)-C(43)	93 (3)
C(11)-Fe(1)-C(13)	106 (2)	C(22)-Fe(2)-C(23)	95 (2)	C(41)-Fe(4)-C(42)	118 (2)	C(42)-Fe(4)-C(44)	121 (2)
C(12)-Fe(1)-C(13)	97 (2)	C(31)-Fe(3)-C(32)	106 (2)	C(41)-Fe(4)-C(43)	98 (3)	C(43)-Fe(4)-C(44)	95 (3)
C(21)-Fe(2)-C(22)	101 (2)	C(31)-Fe(3)-C(33)	100 (2)	C(41)-Fe(4)-C(44)	118 (2)		

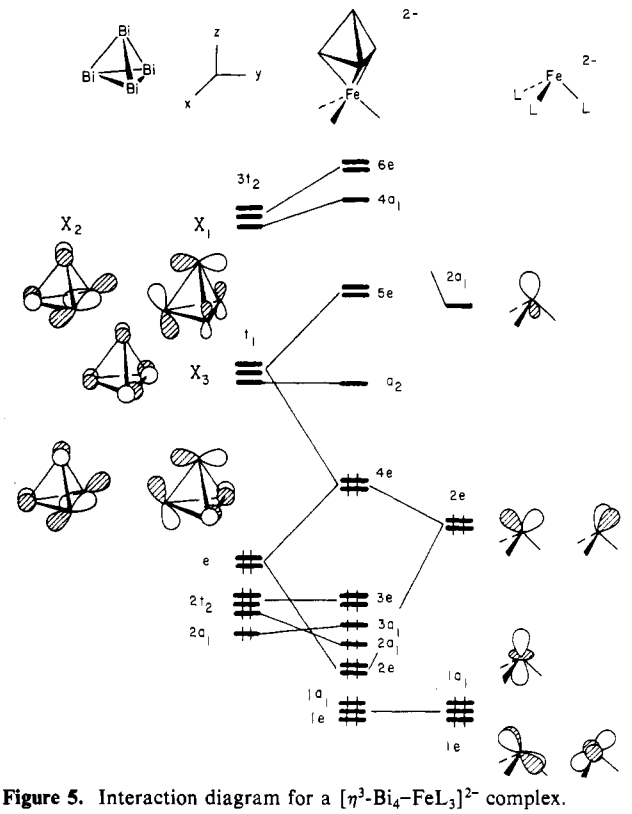

Figure 5. Interaction diagram for a $[\eta^3\text{-}Bi_4\text{-}FeL_3]^{2-}$ complex.

would predict that the coordinated Bi–Bi bonds should be longer than those to the apical Bi atom. This is a result that can be traced to the mixing of the higher lying X_1 and X_2 components of the $3t_2$ set into the 4e MO. These two fragment orbitals are strongly Bi–Bi antibonding between the coordinated Bi atoms, but only weakly so to the apical Bi atom. This effect is important in the cluster compound described in the next section.

The $[Bi_4(\mu_3\text{-}FeL_3)_3]^{2-}$ Cluster Compound. When three C_{3v} ML_3 fragments are combined together in a triangle, each fragment orbital interacts to form an e set and an a_1 or a_2 orbital in the new C_{3v} symmetry. The lower three "t_{2g}-like" orbitals, the $1a_1$ and 1e set on the right side of Figure 2, form nine occupied orbitals. They are all close and low-lying in energy and, therefore, will not behave as valence orbitals or interact strongly with the Bi_4 orbitals. The important valence orbitals in the $(FeL_3)_3$ fragment are derived from symmetry-adapted linear combinations of the three higher orbitals in ML_3, i.e. the $2a_1$ and 2e set. The orbital shapes are shown from a top view in Figure 6. The $1a_1$, 1e, 2e, and a_2 fragment orbitals, which come from the 2e sets of the ML_3 units, are not split much in energy because of long Fe–Fe distances (4.16 Å) in the cluster compound.

Figure 7 represents the interaction diagram for a $(FeL_3)_3^{2-}$ fragment interacting with Bi_4. On the left side of Figure 7 are the orbitals of Bi_4. The X_2 and X_3 components of the $2t_2$ set along with $2a_1$ on Bi_4 are slightly destabilized by the lower lying nine "t_{2g}-like" orbitals. The resultant 2e, $1a_1$, and $2a_1$ MO's are occupied with eight electrons and correspond to Bi lone pairs in the cluster compound. A similar situation occured for the $Bi_4(\mu_3\text{-}ML_3)$ model. The $1a_1$ level on the metal fragment is also basically nonbonding and becomes the HOMO, $3a_1$, in the cluster compound. The e set and the X_1, X_2 components of t_1 on Bi_4 along with 1e and 2e on the metal fragment combine to give four e sets in the molecule, three of which are shown in Figure 7 (1e, 3e, and 4e). The lowest two MO's, 1e and 3e, are Fe–Bi bonding and are filled. They correspond to the 2e, 4e set in Figure 5 for $Bi_4FeL_3^{2-}$. One of the big differences with the μ_3 model is the stabilized, occupied a_2 MO in the cluster. In Figure 5, the a_2 MO is the nonbonding X_3 component of the t_1 set and is the LUMO. However, a symmetry-adapted linear combination of three FeL_3 fragments produces one orbital of a_2 symmetry. This a_2 level

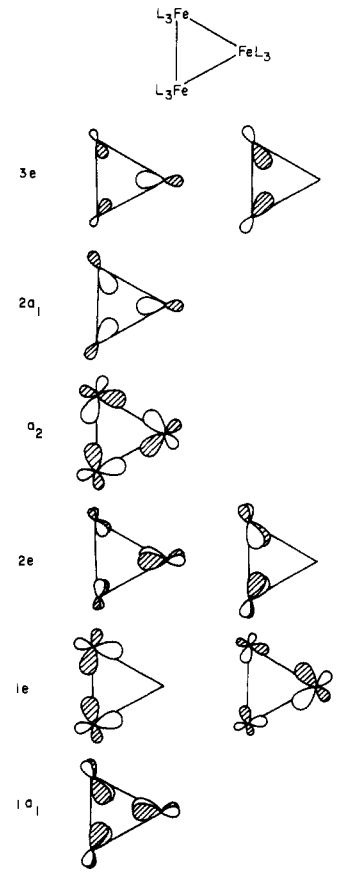

Figure 6. Valence orbitals for an $(ML_3)_3$ fragment.

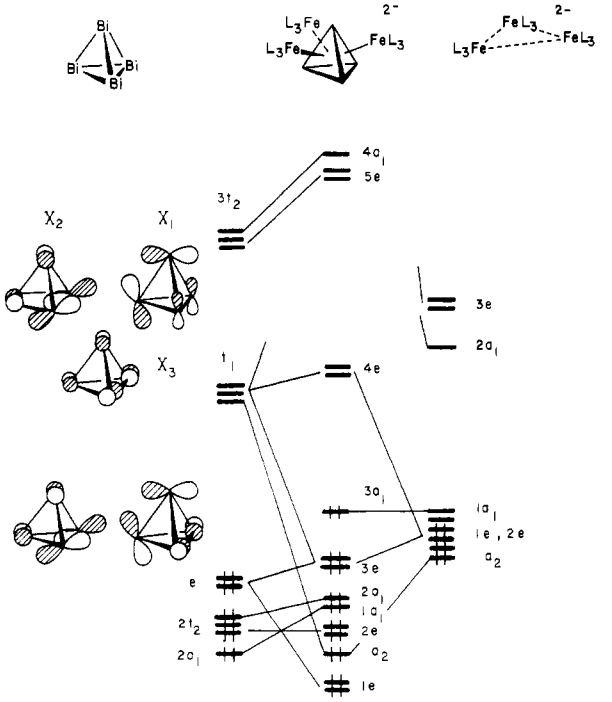

Figure 7. Orbital interaction diagram for the $[Bi_4(\mu_3\text{-}FeL_3)_3]^{2-}$ complex.

strongly interacts with the X_3 component of t_1 to form an occupied, bonding a_2 MO. This interaction is one of the predominant driving forces for bonding in the cluster compound.

Considering the a_2 and 3e MO's there is appreciable backbonding to all components of the empty t_1 set on Bi_4. In our calculations X_1 and X_2 gain 0.57 electrons while X_3 gains 0.63 electrons in t_1. Since these are Bi–Bi antibonding orbitals, their occupation will weaken the Bi–Bi bonds. The e set of Bi_4 is Bi–Bi bonding. Interaction with the metal fragment orbitals (1e and 2e on the right side of Figure 7) causes a redistribution of electron density such that the e set loses 0.80 electrons. This also serves to weaken the Bi–Bi interaction in the cluster. The Bi–Bi overlap populations for the atoms in the noncoordinated face of $Bi_4(FeL_3)_3^{2-}$ are 0.148 larger than the other three (in a calculation where all six Bi–Bi distances are equal to the average value in the experimental structure). This is consistent with the differences observed in the X-ray structure; namely, the basal–basal Bi–Bi distances average 3.157 Å while the apical–basal ones are 3.466 Å. The rationale for the Bi–Bi overlap population difference can be traced to the intervention of the $3t_2$ set on Bi_4 in a way that is analogous to that for $Bi_4FeL_3^{2-}$ as discussed in the previous section.

Each iron atom satisfies the 18-electron rule. Inspection of Figure 7 shows that the molecular 1e, a_2, and 3e levels are Fe–Bi bonding and thus contribute 10 electrons. Likewise, Bi_4 $1a_1$ and the X_1, X_2 components of $1t_2$ (see Figure 4) are stabilized by the $2a_1$ + 3e set on $(FeL_3)_3^{2-}$ (see Figure 6), thus six more electrons are formally donated to the metal. The molecular $3a_1$ and nine "t_{2g}" members are nonbonding and localized on the metal. Finally 18 electrons are donated by the two-electron auxiliary ligands, L, giving a total of 54 electrons assigned to the three Fe atoms.

The cluster $[Bi_4Fe_4(CO)_{13}]^{2-}$ does not obey Wade's rules for a seven-vertex closo cluster since the $Bi_4Fe_3^{2-}$ core contains 10 cluster valence electron pairs and does not adopt the pentagonal-bipyramidal geometry.[14g]

From the opposite perspective, a cluster containing 10 skeletal pairs should be based on a nine-vertex tricapped trigonal prism. Since the $Bi_4Fe_3^{2-}$ core contains only seven vertices, it would be considered an arachno cluster. The observed geometry could be obtained by removing two of the vertices from one of the triangular faces of the trigonal prism and moving the third vertex to lie on the 3-fold axis. It is not obvious from the electron-counting approach why this distortion to C_{3v} symmetry occurs, but it is chemically reasonable since an arachno structure formed by removal of two of the trigonal-prism vertices would contain an $Fe(CO)_3$ unit bridging only two bismuth atoms, a situation that is intuitively not likely to be stable.

It may be more useful here to derive our view of this cluster based on a hypothetical Bi_4 molecule that would have a T_d arrangement of Bi atoms but would possess six skeletal electron pairs and would be, therefore, a nido trigonal bipyramid (one vertex missing). Addition of three $Fe(CO)_3$ units, each of which would function as a two-electron donor, would have the effect of breaking three Bi–Bi bonds, as these electrons would go into antibonding orbitals. The additional two electrons are placed in the molecular $3a_1$ level (see Figure 7), which is essentially Fe–Bi nonbonding. This analysis would, therefore, agree with the observed Bi–Bi basal–basal and basal–apical distances and with the MO results.

As a reviewer has suggested, an alternative electron-counting analysis would be to say that, in addition to the $2a_1$ and $2t_2$ nonbonding orbitals, the $1a_1$ and $1t_1$ orbitals are also highly localized on bismuth and do not, therefore, contribute significantly to Bi–Bi or Bi–Fe bonding. Electron-counting schemes normally neglect the involvement of external lone pairs on main-group elements so that bismuth (five valence electrons) would be classified as a three-electron donor as has been supposed in the discussion to this point; however, each bismuth would have four nonbonding electrons according to this alternate analysis and would function as a one-electron donor. This would give the cluster six "active" skeletal electron pairs compatible with a tricapped tetrahedron. This, however, obscures the issue as to why there are large differences in the Bi–Bi bond distances, and we tend to favor the former analysis.

More recently Teo has proposed a formalism for electron counting in large transition-metal clusters (eq 1).[1b,c,15] Here

$$\text{CVMO} = \frac{N}{2} = 8V - F + 2 \qquad (1)$$

(15) (a) Teo, B. K. *Inorg. Chem.* **1985**, *24*, 115. (b) Mingos, D. M. P. *Inorg. Chem.* **1985**, *24*, 115.

CVMO is the number of cluster valence molecular orbitals, N is the number of cluster valence electrons, V is the number of vertices, and F is the number of faces. It can be shown by similar arguments where main-group elements are involved that the equation becomes

$$\text{CVMO} = 8V_1 + 3V_2 - F + 2 \qquad (2)$$

where V_1 is the number of transition-metal vertices and V_2 is the number of main-group (eight-electron) vertices. This equation predicts 28 CVMO's or 56 cluster valence electrons for the $Bi_4Fe_3^{2-}$ core geometry, and this is what is observed for $Bi_4Fe_3L_9^{2-}$. This counting scheme neglects the low-lying lone pairs on each bismuth and treats bismuth as a three-electron donor to the cluster count. The origin of 54 of the electrons in MO terms has been discussed previously; the additional two electrons come from the X_3 component of $1t_2$ on Bi_4. It will be interesting to see if other large main-group–transition-metal clusters obey this formalism.

Experimental Section

Synthesis of $[Et_4N]_2[Bi_4Fe_4(CO)_{13}]$. The previously described complex $[Et_4N][BiFe_3(CO)_{10}]$ (1.9 g) was dissolved in 100 mL of CH_2Cl_2 and the solution transferred to a 300-mL Parr reactor, which had been purged with dry, oxygen-free N_2. The autoclave was then sealed and purged twice with 500 psi of CO (Matheson) before filling to 500 psi of CO. The solution was either stirred overnight or allowed to stand for several days. In the former case, a powder was formed, and in the latter, crystals were deposited that were suitable for single-crystal X-ray diffraction. After 2 days, the autoclave was vented and the solution as a slurry of the dark black precipitate was transferred quickly to a Schlenk apparatus, filtered, and dried under vacuum. The compound is insoluble in most organic solvents and H_2O but does have appreciable solubility in CH_3CN. IR (ν_{CO}, CH_3CN): 2003 (m), 1960 (vs), 1908 (m) and 1880 (m) cm^{-1}. Anal. Calcd for $C_{29}H_{40}N_2O_{13}Fe_4Bi_4$: C, 20.68; H, 2.39; N, 1.66; Fe, 13.26; Bi, 49.64. Found: C, 18.62; H, 2.31; N, 1.70; Fe, 13.36; Bi, 50.12. The solution from which the title complex was obtained showed the presence of $Fe(CO)_5$.

Collection of X-ray Diffraction Data for $[Et_4N]^+_2[Bi_4Fe_4(CO)_{13}]^{2-}$. The dark brownish-red crystals of $[Et_4N]^+_2[Bi_4Fe_4(CO)_{13}]^{2-}$ were all, unfortunately, rather platelike. The crystal selected for the X-ray diffraction study had the approximate dimensions $0.3 \times 0.3 \times 0.13$ mm^3. It was sealed in a thin-walled glass capillary and was mounted and accurately aligned in a eucentric goniometer on the Syntex $P2_1$ automated four-circle diffractometer. All subsequent setup operations (i.e., determination of unit cell parameters, crystal orientation matrix, and Laue group) were carried out as described previously.[16] Intensity data were collected via the ω-scan routine[17] because of the unusually long c axis (~40 Å); details are given in Table I. The systematic absences ($0kl$ for $l = 2n + 1$, $h0l$ for $h = 2n + 1$ and $hk0$ for $k = 2n + 1$) uniquely define the centrosymmetric orthorhombic space group *Pcab* (a nonstandard setting of *Pbca*, No. 61).[18] All diffraction data were corrected for absorption and for Lorentz and polarization effects. All data were reduced to unscaled $|F_o|$ values, which were then placed on an absolute scale by means of a Wilson plot.

Solution of the Crystal Structure of $[Et_4N]^+_2[Bi_4Fe_4CO)_{13}]^{2-}$. All crystallographic calculations were performed on our in-house Syntex XTL system consisting of a Data General NOVA 1200 computer (with parallel floating-point processor), a Diablo disk unit, and a Versatec printer/plotter with the SUNY—Buffalo-modified version of the XTL interactive crystallographic program package. The analytical form of the scattering factor for the appropriate neutral atoms was used in calculating F_c values; these were corrected for both the real ($\Delta f'$) and imaginary ($\Delta f''$) components of anomalous dispersion.[19]

Table V. Parameters Used in the Extended Hückel Calculations

atom	orbital	H_{ii}, eV	ζ_1	ζ_2	C_1[a]	C_2[a]
Fe	3d	−12.70	5.35	1.80	0.5366	0.6678
	4s	−9.17	1.90			
	4p	−5.37	1.90			
Bi	6s	−15.75	2.6531			
	6p	−10.52	2.0923			
C	2s	−21.40	1.625			
	sp	−11.40	1.625			
O	2s	−32.30	2.275			
	2p	−14.80	2.275			
H	1s	−13.60	1.30			

[a] Contraction coefficients used in the double-ζ expansion.

The function minimized in the least-squares refinement processes was $\Sigma w(|F_o| - |F_c|)^2$, where $1/w = [\sigma(|F_o|)^2] + (0.05|F_o|)^2$.

The structure was solved by direct methods (using MULTAN).[20] The four bismuth atoms were located from an initial "*E* map"; the remainder of the non-hydrogen atoms were located from a succession of difference Fourier maps. The two $[Et_4N]^+$ ions were found to be disordered, but the focal $[Bi_4Fe_4(CO)_{13}]^{2-}$ ion is ordered. Refinement of positional and thermal parameters (anisotropic only for the Bi_4Fe_4 moiety) of all non-hydrogen atoms led to convergence with[21] $R_F = 7.8\%$, $R_{wF} = 9.4\%$, and GOF = 1.30 for those 2926 reflections with $|F_o| > 3.0\sigma(|F_o|)$ and $R_F = 6.1\%$, $R_{wF} = 8.0\%$, and GOF = 1.24 for those 2343 reflections with $|F_o| > 6.0\sigma(|F_o|)$.

A final difference Fourier map revealed no unexpected features; the structure is thus complete. Final position and thermal parameters are collected in Table II.

Molecular Orbital Calculations. The calculations have been carried out with the extended Hückel formalism[22] using the weighted H_{ij} formula.[23] The H_{ij}'s of the Bi atom were taken from an extrapolation for group 15 elements.[24] The orbital exponents of the Bi atom were from Fitzpatrick and Murphy.[25] The other parameters were obtained from previous work.[26] The atomic parameters are listed in Table V. In the molecular model, L is a two-electron donor, i.e. CO or H^-. All Bi–Bi, Fe–Bi, Fe–C, Fe–H, and C–O bond lengths were set at 3.466, 2.72, 1.78, 1.60, and 1.14 Å, respectively. The L–Fe–L angles were fixed at 90.0°.

Acknowledgment. This work was supported by the Robert A. Welch Foundation, the donors of the Petroleum Research Fund, administered by the American Chemical Society, and the National Science Foundation (Grant CHE-8421217). The high-pressure equipment that made this study possible was provided from the Research Corp. through a grant from the Atlantic Richfield Foundation. T.A.A. is an Alfred P. Sloan Research Fellow.

Registry No. I, 94483-21-3; II, 92786-73-7; Bi, 7440-69-9; Fe, 7439-89-6.

Supplementary Material Available: A table of anisotropic thermal parameters (1 page). Ordering information is given on any current masthead page.

(16) Churchill, M. R.; Lashewycz, R. A.; Rotella, F. J. *Inorg. Chem.* **1977**, *16*, 265.
(17) Churchill, M. R.; Lashewycz, R. A. *Inorg. Chem.* **1978**, *17*, 1950.
(18) *International Tables for X-Ray Crystallography*; Kynoch: Birmingham, England, 1965; Vol. 1, pp 150 and 548.
(19) *International Tables for X-Ray Crystallography*; Kynoch: Birmingham, England, 1974; Vol. 4, pp 99–101 and 149–150.
(20) (a) Germain, G.; Wolfson, M. M. *Acta Crystallogr., Sect. B: Struct. Crystallogr. Cryst. Chem.* **1968**, *B24*, 91. (b) Germain, G.; Main, P.; Woolfson, M. M. *Acta Crystallogr., Sect. A: Cryst. Phys., Diffr., Theor. Gen. Crystallogr.* **1971**, *A27*, 368.
(21) R_F (%) = $100\Sigma||F_o| - |F_c||/\Sigma|F_o|$, R_{wF} (%) = $100[\Sigma w(|F_o| - |F_c|)^2/\Sigma w|F_o|^2]^{1/2}$, and GOF = $[\Sigma w(|F_o| - |F_c|)^2/(NO - NV)]^{1/2}$, where NO = number of observations and NV = number of variables.
(22) Hoffmann, R. *J. Chem. Phys.* **1963**, *39*, 1397. Hoffmann, R.; Lipscomb, W. N. *J. Chem. Phys.* **1962**, *36*, 2179, 3489; **1962**, *37*, 2872.
(23) Ammeter, J. H.; Burgi, H.-B.; Thibeault, J. C.; Hoffmann, R. *J. Am. Chem. Soc.* **1978**, *100*, 3686.
(24) Huzinaga, S. *Gaussian Basis Sets for Molecular Calculations*; Elsevier Science: Amsterdam, 1984.
(25) Fitzpatrick, N. J.; Murphy, G. H. *Inorg. Chim. Acta* **1984**, *87*, 41.
(26) Albright, T. A.; Hofmann, P.; Hoffmann, R. *J. Am. Chem. Soc.* **1977**, *99*, 7546.